



Fabrication and Characterization of Fully Flattened Carbon Nanotubes: A New Graphene Nanoribbon Analogue

D. H. Choi¹, Q. Wang¹, Y. Azuma², Y. Majima², J. H. Warner³, Y. Miyata¹, H. Shinohara¹ & R. Kitaura¹

¹Department of Chemistry, Nagoya University, Nagoya, 464-8602, Japan, ²Materials and Structures Laboratory, Tokyo Institute of Technology, Yokohama 226-8503, Japan, ³Department of Materials, University of Oxford, Paris Road, Oxford OX1 3PH, United Kingdom.

SUBJECT AREAS:

SYNTHESIS OF
GRAPHENE

NANOSCALE MATERIALS

SYNTHESIS AND PROCESSING

ELECTRONIC PROPERTIES AND
DEVICES

Received

8 January 2013

Accepted

22 March 2013

Published

8 April 2013

Correspondence and requests for materials should be addressed to H.S. (noris@nagoya-u.jp) or R.K. (r.kitaura@nagoya-u.jp)

Graphene nanoribbons (GNR) are one of the most promising candidates for the fabrication of graphene-based nanoelectronic devices such as high mobility field effect transistors (FET). Here, we report a high-yield fabrication of a high quality another type of GNR analogue, fully flattened carbon nanotubes (flattened CNTs), using solution-phase extraction of inner tubes from large-diameter multi-wall CNTs (MWCNTs). Transmission electron microscopy (TEM) observations show that flattened CNTs have width of typically 20 nm and a barbell-like cross section. Measurements of the low-bias conductance of isolated flattened CNTs as a function of gate voltage shows that the flattened CNTs display ambipolar conduction which is different from those of MWCNTs. The estimated gap based on temperature dependence of conductivity measurements of isolated flattened CNTs is 13.7 meV, which is probably caused by the modified electronic structure due to the flattening.

Graphene have been extensively studied due to their fascinating electrical, optical and mechanical properties^{1–3}. In particular, graphene-based electronics have attracted much attention due to high carrier mobility: $> 10,000 \text{ cm}^2\text{V}^{-1}\text{s}^{-1}$ at room temperature. In addition, atomically thin structure of graphene provides the possibility of fabricating high speed devices with ultrathin and short channels without suffering from the adverse short-channel effects⁴. One of the main issues for the future graphene-based electronics is the fact that the graphene is zero-gap semiconductors, so that the opening of a sizable and well-defined bandgap is the key factor for the successful construction of such brand-new electronics.

Several different ways to open bandgap have so far been proposed such as the electronic field induced gap opening of bilayer graphene and the symmetry breaking of graphene sublattice resulting from interaction between the graphene layer and the substrates^{5,6}. Among the proposed ways to open bandgap in graphene, graphene width confinement down to several tens of nanometer, that is fabrication of graphene nanoribbon (GNR), has attracted attentions as the most promising and straightforward way to provide band gaps^{7,8}. Although many researches have already fabricated GNRs incorporating such as unzipping of CNTs, templated growth on SiC and the narrowing of width of graphene by electron beam lithography, the reproducible and efficient production of GNRs is still difficult and important issue^{9–12}. Here, we report a brand-new and simple approach producing high quality GNR analogues, what we call fully flattened carbon nanotubes (FNT), using solution-base extraction of inner tubes from large-diameter multi-wall CNTs (MWCNTs).

The schematic representation of the production mechanism is shown in Figure 1, where extracted large-diameter CNTs are spontaneously flattened to form FNTs. The structure of FNT is almost identical to that of GNRs except for the edges: smooth and round shaped edge of FNTs and defective and open edge of GNRs. The first experimental identification of FNTs was done by Zettl and coworkers when they were looking at MWCNTs by a TEM¹³. The advantage of our method is the simple and easy preparation only via solution phase sonication/extraction of high-quality MWCNTs.

Results

Sample preparation and structure characterization. MWCNT synthesized by arc-discharge (Aldrich Inc., Bucky tube) was used in this experiment without further purification. Figure 2a show TEM images of the MWCNTs used in this experiment. The TEM images clearly show that the MWCNTs sample is clean without impurities such as metal nanoparticles. Typical diameter and layer number of the MWCNTs obtained from

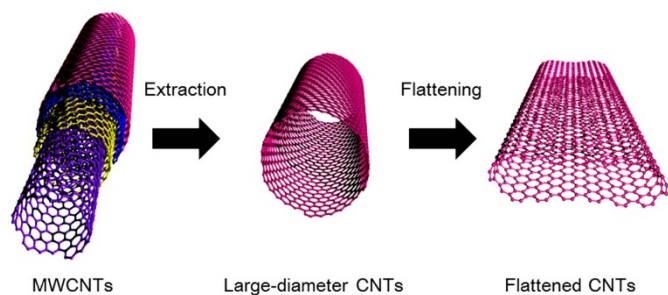


Figure 1 | A schematic representation of the preparation procedure of flattened CNTs. The large-diameter CNT is extracted from MWCNT, and the extracted CNT is spontaneously flattened to form FNT.

high-magnification images were 13 nm and 5, respectively. As clearly seen in the TEM images, walls of the MWCNTs are straight having high crystallinity without any kinks. As discussed later, the high crystallinity of MWCNTs is essential to produce FNTs from MWCNTs.

Prior to the extraction of large-diameter CNTs, caps existing at both ends of MWCNT were removed by heating the sample at 973 K for 30 min under dry air flow. This heating causes weight loss of typically 40%, which ensures the complete removal of the MWCNT caps. After removal of the caps, we sonicated the sample in 1,2-dichloroethane or water containing surfactant for typically 1 hours (Supplementary Fig. S1, S2). Figure 2b shows TEM image of the sample after the sonication process. As clearly illustrated in the images, typical diameter and wall number of the sample are significantly different from those of the original MWCNTs; the typical diameter and wall number of the sample after the sonication were 20 nm and 2 ~ 3, respectively. In addition, we can find a twisted structure as seen at the bottom right of Fig 2b (marked by the arrow). Formation of this kind of twisted structure is not compatible with the structure of MWCNTs. In fact, such a twisted structure has never been found in the original MWCNTs sample. The observed marked difference of TEM images indicates that the sonication induces not only a dispersion of sample into solution but also significant modification of the structure of MWCNTs.

Figure 3 shows high magnification aberration-corrected TEM image and the corresponding fast Fourier Transform (FFT) image of the sample after the sonication. The TEM image shows two liner contrasts at both edges, which is similar to the folded edge of bilayer graphene; the edge is visible by the (002) graphene lattice fringe in the case of folded graphene. Moiré pattern is clearly seen, which originates from a superposition of the hexagonal network of graphene layers. The FFT image shows four sets of hexagonal pattern that is marked by red, green, pink and yellow hexagon in the figure. These four sets of hexagonal pattern mean that the number of graphene layer is at least four, which is consistent to the folded bilayer of

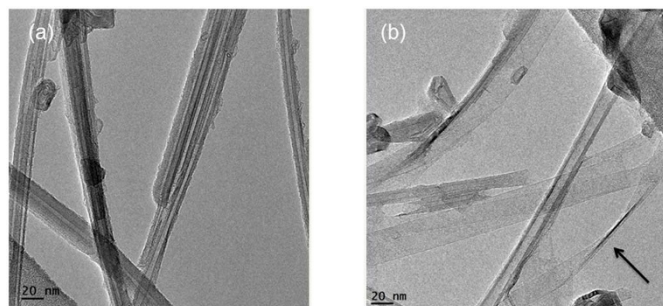


Figure 2 | TEM images of the MWCNTs (a) before and (b) after the solution-based sonication process. The twisted structure is marked by the arrow.

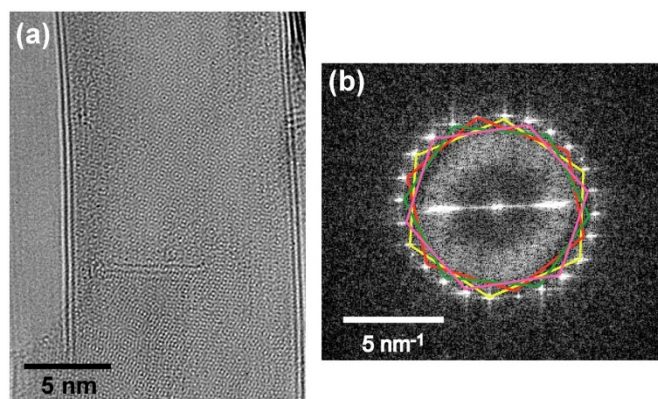


Figure 3 | (a) a high-resolution TEM image of an isolated FNT taken by aberration-corrected TEM, (b) FFT image of the image (a).

graphene. In addition, two pairs of the hexagonal patterns (red and yellow, green and pink) have 2 mm symmetry, indicating that the orientation of the graphene layers is not random. The electron diffraction patterns and FFT of atomically resolved TEM images of a single-wall CNT (SWCNT) under normal incidence always have 2 mm symmetry, which results from the mutual orientation of face-to-face graphene layers in SWCNTs¹⁴. So, the observed 2 mm symmetry of the FFT images indicates that the interlayer orientation of CNTs does not change after the sonication process. Based on the mutual orientation of the hexagons in the FFT image (red and yellow, green and pink hexagons), chiral angles of the original SWCNTs were estimated to be 9.5 and 24.8 degree. Assuming the flattened CNTs having the chiral angles, the TEM image shown in Fig. 3a have been reproduced by the multi-slice-method based TEM image simulation (supplementary Fig. S3). To further investigate this structural change, cross-sectional image of the material was observed (Figure 4). As clearly seen in the image, the cross section is not circular but a planar with rounded structures at both ends, suggesting that the resulting material is not CNTs or GNRs but flattened CNTs (FNTs). It is worth noting that the obtained TEM images of the FNTs sample are identical to the previously reported TEM images of samples prepared by sonication-based unzipping of CNTs¹⁵. This means that we have to be careful to characterize the structure of samples prepared by sonication of CNTs.

Electronic properties of FNTs. The deformation of CNTs can alter their electronic properties. To investigate electronic properties of

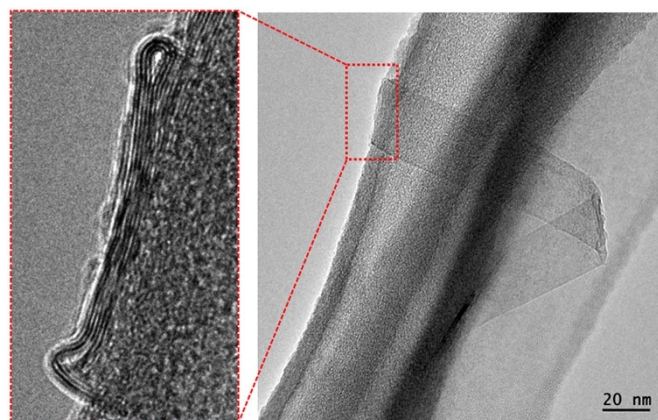


Figure 4 | Right-side image: a TEM image of a FNT wrapping around carbon membrane of a TEM grid, left-side image: close-up of the red square shown in the TEM image showing a barbell-like cross section of FNT.



FNTs, we made electrical contacts to several individual FNTs using electron beam lithography. Inset in Fig. 5 shows typical AFM image of the so-prepared FNT device. The electrical contact was made using Ti/Au with thickness of 5 and 45 nm. All experiments in this report were performed on back-gated FNTs on a substrate of highly doped silicon with a 90 nm thick SiO₂ gate dielectric. Figure 5 shows an example of transfer characteristic of the FNT device with a FNT channel length of 600 nm measured at ten different temperatures ranging from 9 to 300 K. The observed transfer characteristic exhibits a typical ambipolar transport behavior with a Dirac point, showing both hole and electron accumulation regime at low gate voltages (−13 ~ 13 V). It should be mentioned that the MWCNTs are supposed to be metallic and to show no gate-voltage dependence. Furthermore, MWCNTs device with a similar geometry shows negligible gate voltage dependence (Supplementary Fig. S4), which clearly indicates metallicity of MWCNTs.

To evaluate the transport gap of FNTs, we have investigated the thermal activation energy by measuring G_{\min} , the minimum conductance observed at Dirac point, at different temperatures. At high temperatures, thermal activation is predominant, and G_{\min} is well represented by the following formula: $G_{\min} \propto \exp(-E_a/2k_B T)$. Activation energy E_a obtained from an Arrhenius plot of G_{\min} was 13.7 meV (Supplementary Fig. S6), which is comparable to the reported values of GNRs prepared by electron-beam lithography¹⁶. The transport gap found in GNRs prepared by lithography is caused by localized states due to disordered edge structure of GNRs¹⁶. In contrast, the FNTs possess smooth and straight edges, which indicate that the observed transport gap is intrinsic characteristic of FNTs caused by the flattening deformation. The observed deformation-induced opening of gap is consistent with the previous study on deformed double-wall CNTs using scanning tunneling microscopy and spectroscopy¹⁷.

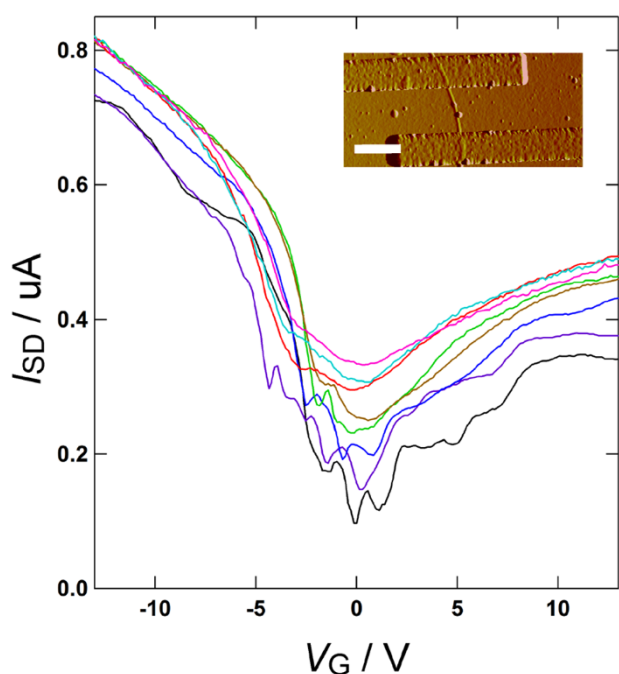


Figure 5 | Transfer characteristics of isolated FNT measured at different temperatures. Drain bias of 100 mV was applied through the measurement. Black, purple, blue, aqua, green, brown and red line correspond to transfer characteristics measured at 9, 60, 100, 140, 180, 220, 260 and 300 K, respectively. The inset shows a typical AFM image of an isolated FNT device, and the scale bar shown in the inset corresponds to 600 nm.

Discussion

Previous theoretical works have shown that tubular shape is structurally less stable than flattened shape when diameter of CNTs becomes large. In this case, tubular structure corresponds to a metastable state¹⁸. Because the tubular structure is a metastable, external stimuli can cause structural transition from the tubular to the flattened structure. A stimuli such as sonication can thus trigger the flattening deformation. The driving force of this structural transformation is the attractive van der Waals force exerted between tube walls of CNTs. When the diameter of CNTs is large enough, the attractive interaction between layers become predominant and the energy gain resulting from the interlayer interaction overcomes the energy loss due to the formation of curvature at the both ends of FNTs. A recent work shows that the minimum diameter inducing the flattening deformation is about 3~5 nm, which is much smaller than that of typical diameter of MWCNTs used in this work^{18,19}. The obtained results indicate that the extraction of large-diameter few-layer CNTs from MWCNTs occurs during the sonication process that finally leads to the formation of FNTs.

Figure 6 presents a TEM image showing the formation process of few-layer large-diameter CNTs from MWCNTs. A large-diameter CNTs (12.1 nm) is obtained after the inner tube extraction from MWCNTs, and the large-diameter CNT is spontaneously flattened to possess width of 18.2 nm that is larger than the outer diameter of original MWCNTs. The ratio between width of the FNT region and outer-diameter of original MWCNTs is 1.6, which is consistent to the expected value of $\pi/2$ (1.57); this value was calculated based on a simple assumption that circular cross section of MWCNTs turned to be straight double layer cross section of FNT. The TEM image clearly demonstrates that the formation of FNT through the extraction of large-diameter CNT from MWCNT.

To investigate the extraction mechanism of few-layer large-diameter CNTs further, a TEM-based statistical analysis of diameter of the original MWCNTs and width of synthesized FNTs was performed. Figure 7 is a histogram showing the distribution of the width of FNTs and the diameter of original MWCNTs; we have counted more than eighty MWCNTs and FNTs to make this histogram. As clearly seen, the width of FNTs is larger than the diameter of MWCNTs, where the average width of FNTs and the average diameter of MWCNTs are 21 and 17 nm, respectively. The average width of FNTs is larger than the average diameter of MWCNTs that is also consistent with the flattening deformation. Shape of the width distribution of FNTs and diameter distribution of MWCNTs are similar each other (standard deviations of each profile are 8.9 and

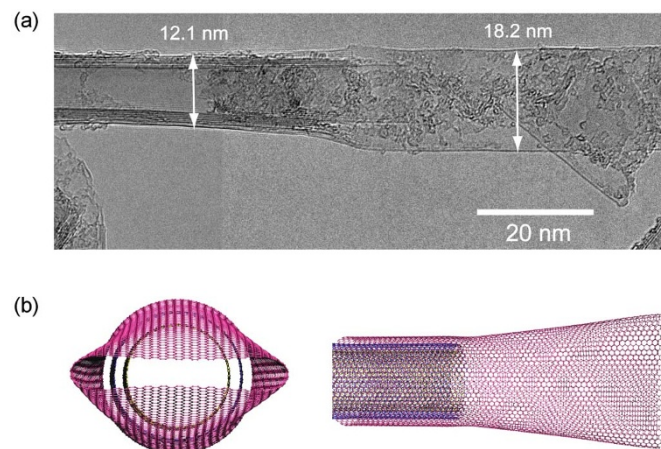


Figure 6 | (a) TEM image showing the extraction process of a large-diameter CNT from a MWCNT. The extracted large-diameter CNT is spontaneously flattened to have a width larger than the diameter of the original MWCNT. (b) Schematic representation of the extraction process.

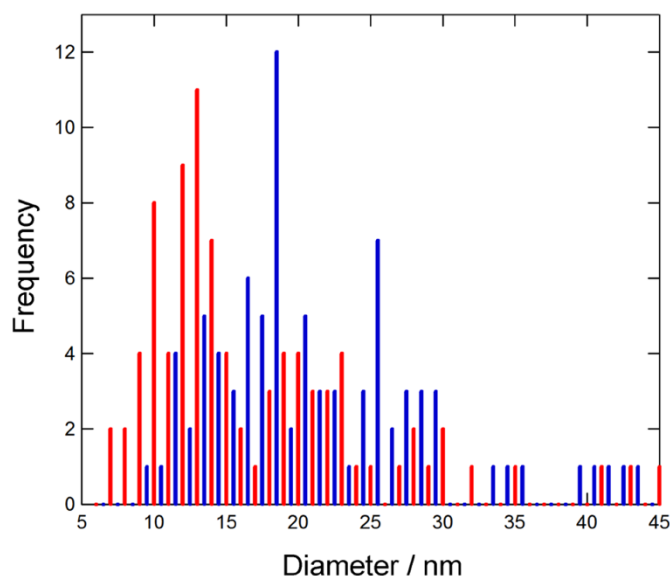


Figure 7 | A histogram showing a diameter distribution of FNTs and MWCNTs. Red and blue bars show the distribution of MWCNT and FNT, respectively.

10 nm respectively), indicating that the extraction of large-diameter CNTs occurs regardless of the diameter of the original MWCNTs.

Previous theoretical and experimental studies on sliding of shells in MWCNTs have shown that friction force between the shells is quite low leading to small energy barrier for the sliding motion²⁰. Due to the small energy barrier, the sliding can be triggered by the shock waves formed under the sonication, which results in the extraction of the outer shell from MWCNTs. This is essentially the same mechanism as the separation of inner and outer tube of DWCNTs that we reported previously²¹. The energy barrier may vary depending on the crystallinity of MWCNTs; when walls of MWCNTs are not straight with kinked structures, the energy barrier is considered to be large. In fact, we could not obtain any FNTs when we use defective MWCNTs as a precursor even after longtime sonication in solution (Supplementary Fig. S7). This means that the high quality MWCNT precursor is required to realize bulk production of FNTs by the solution phase extraction technique.

While structure of FNTs has features in common with multiply-folded graphene (multiply-stacked graphene layers and folded edges for example), there are essential differences in structure between FNTs and multiply-folded graphene²². Structure of multiply-folded graphene is basically two-dimensional, which is in contrast to the one-dimensional structure of FNTs where folded edges are typically separated by 10 ~ 20 nm. Compared to multiply-folded graphenes, FNTs can therefore show electronic properties arising from one-dimensionality, and electronic structure modifications originating from folded edges are expected to be more significant. As discussed in the results part, FNTs device shows transport gap. There are two probable reasons why the gap appears in FNTs: the presence of curvature at both edges of FNTs and the interlayer interaction between neighboring graphene sheets. A theoretical calculation on folded graphene shows that bandgap appears in several different mutual orientations of graphene²³. This bandgap opening is attributed to hybridization of the π electron states between the upper and lower layers of the folded graphene. The interlayer interaction depends on the orientation of graphene layers. Due to computational limitations, the theoretical investigation of the interlayer interaction is limited to the orientation close to the so-called AA stacking. The high degree of curvature at edges induces a strong deformation in carbon sigma bonds, and thus leads to the valence charge modification²⁴. FNTs synthesized in this work are relatively thin (average

width is 18 nm) and possess such curvatures at both edges, and therefore, the electronic structure of the whole FNTs can be greatly affected by the curvature formation. This kind of electronic structure modification could be one of the main reasons why gap appears in this system²⁵. In addition, the curvature leads to shifts of the Fermi point away from the K-point of the Brillouin zone, which modifies the low-energy electronic states²⁶. This can cause change of the first van Hove singularities position that can also induce the bandgap. Further investigation based on correlation between exact structure of FNTs and electronic properties will be definitely needed to fully understand the electronic properties of FNTs.

In conclusion, we have successfully developed a new synthesis method of FNTs in bulk scale based on a simple solution phase dispersion process, where FNTs are formed by the spontaneous flattening of extracted large-diameter few-layer CNTs. The flattened structure of FNTs is characterized by TEM observations, and FET device measurements using single isolated FNT shows an ambipolar characteristic. Temperature dependence of G_{\min} shows the transport gap of 13.7 meV, which is probably caused by the modified electronic structure due to the flattening. The present method can be scaled up for large-scale production of GNR-analogue materials, which is potentially useful for future electronics and basic researches on deformed graphene systems.

Methods

Preparation of samples. The MWCNT-sample was supplied from Aldrich Inc. and used without further purification. Prior to the extraction of large-diameter CNTs, closed edges existing at both ends of MWCNT were etched away by a thermal oxidation reaction at 973 K for 30 min under dry air flow. Weight loss of the MWCNT during the oxidation process was monitored by thermal gravimetric analyses (TGA, example of the TGA is shown in Supplementary Fig. S8). A typical weight loss after the oxidation process is 40%, which ensures the complete opening of closed caps of the MWCNT. For the extraction of large-diameter CNTs, the MWCNTs sample (7 mg) was dispersed in 1,2-dichloroethane or H₂O (20 mL) with 1% weight per volume (w/v) solution of sodium cholate hydrate (SC, 99% Sigma-Aldrich) using an ultrasonic sonicator (Sonifire 450D, Branson) for 1 h at 298 K. Obtained dispersion solution was centrifuged for 1 hour at 41,000 g and supernatant solution was collected (pictures of the dispersion solution are shown in Supplementary Fig. S9). The supernatant solution was mixed with methanol, and precipitated FNT was collected by filtration.

TEM observations. TEM observations were carried out using a high-resolution field-emission gun TEM (JEM-2100F and JEM-2200MCO, JEOL) operated at 80 keV at room temperature and under a pressure of 10^{-6} Pa. Atomic resolution TEM (Figure 3), was performed using a JEOL 2200MCO, fitted with CEOS image and probe aberration correctors, operating at 80 kV. The sample was dispersed in DCE by the weak sonication for 1 hour with an ultrasonic bath sonicator. The solution was then dropped onto a Si grid or copper grid coated with thin carbon film. The sample was heated at 200°C under vacuum for 30 min to remove DCE and water just before the TEM observations. TEM images were recorded with a charge coupled device with an exposure time of typically 1 s.

Measurements of electronic properties. FNTs were deposited on a heavily doped silicon substrate with a 90 nm thick SiO₂ layer by spin-coating. First, the FNTs dispersed in DCE solution was dropped onto the substrate and leave it for 5 min. And then, the solution was spin-coated at 4000 rpm for 1 min. The location of FNTs was determined using atomic force microscope (Dimension 3100 SPM, Veeco) based on pre-fabricated marks on the substrate. Electric contacts of Ti (5 nm)/Au (45 nm) were made using electron beam lithography (ELS-7500EX, ELIONIX) and electron beam evaporator (E-400EBS, SHIMADZU). Transfer and output characteristics of FNTs device were performed using a vacuum probe station (Nagase) and semiconductor parameter analyzer (B1500, Agilent).

- Novoselov, K. S. *et al.* Two-dimensional gas of massless Dirac fermions in graphene. *Nature* **438**, 197–200 (2005).
- Bae, S. *et al.* Roll-to-roll production of 30-inch graphene films for transparent electrodes. *Nat Nanotechnol* **5**, 574–578 (2010).
- Bunch, J. S. *et al.* Electromechanical resonators from graphene sheets. *Science* **315**, 490–493 (2007).
- Liao, L. *et al.* Sub-100 nm Channel Length Graphene Transistors. *Nano Lett.* **10**, 3952–3956 (2010).
- Ohta, T., Bostwick, A., Seyller, T., Horn, K. & Rotenberg, E. Controlling the electronic structure of bilayer graphene. *Science* **313**, 951–954 (2006).
- Zhou, S. Y. *et al.* Substrate-induced bandgap opening in epitaxial graphene. *Nature Materials* **6**, 916–916 (2007).



7. Han, M. Y., Ozyilmaz, B., Zhang, Y. B. & Kim, P. Energy band-gap engineering of graphene nanoribbons. *Phys. Rev. Lett.* **98**, 206805 (2007).
8. Son, Y. W., Cohen, M. L. & Louie, S. G. Energy gaps in graphene nanoribbons. *Phys. Rev. Lett.* **97**, 216803 (2006).
9. Bai, J. W., Duan, X. F. & Huang, Y. Rational Fabrication of Graphene Nanoribbons Using a Nanowire Etch Mask. *Nano Lett.* **9**, 2083–2087 (2009).
10. Kosynkin, D. V. *et al.* Longitudinal unzipping of carbon nanotubes to form graphene nanoribbons. *Nature* **458**, 872–U875 (2009).
11. Jiao, L. Y., Zhang, L., Wang, X. R., Diankov, G. & Dai, H. J. Narrow graphene nanoribbons from carbon nanotubes. *Nature* **458**, 877–880 (2009).
12. Sprinkle, M. *et al.* Scalable templated growth of graphene nanoribbons on SiC. *Nat Nanotechnol* **5**, 727–731 (2010).
13. Chopra, N. G. *et al.* Fully Collapsed Carbon Nanotubes. *Nature* **377**, 135–138 (1995).
14. Qin, L. C. Electron diffraction from carbon nanotubes. *Rep. Prog. Phys.* **69**, 2761–2821 (2006).
15. Jiao, L. Y., Wang, X. R., Diankov, G., Wang, H. L. & Dai, H. J. Facile synthesis of high-quality graphene nanoribbons. *Nat Nanotechnol* **5**, 321–325 (2010).
16. Han, M. Y., Brant, J. C. & Kim, P. Electron Transport in Disordered Graphene Nanoribbons. *Phys. Rev. Lett.* **104**, – (2010).
17. Giusca, C. E., Tison, Y. & Silva, S. R. P. Evidence for Metal-Semiconductor Transitions in Twisted and Collapsed Double-Walled Carbon Nanotubes by Scanning Tunneling Microscopy. *Nano Lett.* **8**, 3350–3356 (2008).
18. Zhang, C. G. *et al.* Closed-Edged Graphene Nanoribbons from Large-Diameter Collapsed Nanotubes. *Acs Nano* **6**, 6023–6032 (2012).
19. Motta, M., Moissala, A., Kinloch, I. A. & Windle, A. H. High performance fibres from ‘Dog bone’ carbon nanotubes. *Adv. Mater.* **19**, 3721–+ (2007).
20. Kis, A., Jensen, K., Aloni, S., Mickelson, W. & Zettl, A. Interlayer forces and ultralow sliding friction in multiwalled carbon nanotubes. *Phys. Rev. Lett.* **97** (2006).
21. Miyata, Y. *et al.* Solution-Phase Extraction of Ultrathin Inner Shells from Double-Wall Carbon Nanotubes. *Acs Nano* **4**, 5807–5812 (2010).
22. Kim, K. *et al.* Multiply folded graphene. *Phys. Rev. B* **83** (2011).
23. Takagi, Y. & Okada, S. Asymmetrical Electronic Structure of Folded Graphene. *J. Phys. Soc. Jpn.* **79**, 033702 (2010).
24. Dumitrica, T., Landis, C. M. & Yakobson, B. I. Curvature-induced polarization in carbon nanoshells. *Chem. Phys. Lett.* **360**, 182–188 (2002).
25. Martel, R., Schmidt, T., Shea, H. R., Hertel, T. & Avouris, P. Single- and multi-wall carbon nanotube field-effect transistors. *App. Phys. Lett.* **73**, 2447–2449 (1998).
26. Lammert, P. E., Zhang, P. H. & Crespi, V. H. Gapping by squashing: Metal-insulator and insulator-metal transitions in collapsed carbon nanotubes. *Phys. Rev. Lett.* **84**, 2453–2456 (2000).

Acknowledgements

This work has been supported by the Grant-in-Aids for Specific Area Research (Grant No. 19084008) on Carbon Nanotube Nano-Electronics and for Scientific Research S (No. 22225001) of MEXT of Japan.

Author contributions

D.H.C. performed the synthesis of the sample. D.H.C., R.K. and J.H.W. performed TEM experiments. D.H.C. and Y.A. fabricated devices and measured the FNT characteristics. R.K. and H.S. designed the study and co-wrote the paper. All authors discussed the results.

Additional information

Supplementary information accompanies this paper at <http://www.nature.com/scientificreports>

Competing financial interests: The authors declare no competing financial interests.

License: This work is licensed under a Creative Commons Attribution-NonCommercial-NoDerivs 3.0 Unported License. To view a copy of this license, visit <http://creativecommons.org/licenses/by-nc-nd/3.0/>

How to cite this article: Choi, D.H. *et al.* Fabrication and Characterization of Fully Flattened Carbon Nanotubes: A New Graphene Nanoribbon Analogue. *Sci. Rep.* **3**, 1617; DOI:10.1038/srep01617 (2013).